

***PPP2R4* dysfunction promotes *KRAS*-mutant lung adenocarcinoma development and mediates opposite responses to MEK and mTOR inhibition**

Bob Meeusen^{1,2}, Emanuela Elsa Cortesi³, Judit Domènech Omella^{1,2}, Anna Sablina^{4,2}, Juan-Jose Ventura³, Veerle Janssens^{1,2*}

¹ Laboratory of Protein Phosphorylation & Proteomics, Dept. Cellular & Molecular Medicine, KU Leuven, B-3000 Leuven, Belgium

² KU Leuven Cancer Institute (LKI), B-3000 Leuven, Belgium

³ Translational Cell & Tissue Research, Dept. Imaging & Pathology, KU Leuven, B-3000 Leuven, Belgium

⁴ Laboratory for Mechanisms of Cell Transformation, VIB Center for Cancer Biology & Dept. Oncology, KU Leuven, B-3000 Leuven, Belgium

Running title: *PPP2R4* in *KRAS*-mutant NSCLC etiology and therapy outcome

*Corresponding author: Prof. V. Janssens, GHB O&N1, Herestraat 49, PO-box 901, B-3000 Leuven, Belgium; email: veerle.janssens@kuleuven.be; phone: +32 16 330 684

Word count: 3760

Number of figures and tables: 8

This manuscript includes supplementary data.

1 **Abstract**

2 *KRAS*-mutant lung adenocarcinomas represent the largest molecular subgroup of non-small
3 cell lung cancers (NSCLC) and are notorious for their dismal survival perspectives. To gain
4 more insights in etiology and therapeutic response, we focused on the tumor suppressor
5 Protein Phosphatase 2A (PP2A) as a player in *KRAS* oncogenic signaling. We report that the
6 PP2A activator PTPA (encoded by *PPP2R4*) is commonly affected in NSCLC by heterozygous
7 loss and low-frequent loss-of-function mutation, and this is specifically associated with
8 poorer overall survival of *KRAS*-mutant lung adenocarcinoma patients. Reduced or mutant
9 *PPP2R4* expression in A549 cells increased anchorage-independent growth *in vitro* and
10 xenograft growth *in vivo*, correlating with increased Ki67 and c-MYC expression. Moreover,
11 *KrasG12D*-induced lung tumorigenesis was significantly accelerated in *Ppp2r4* gene trapped
12 mice as compared to *Ppp2r4* wild-type. A confined kinase inhibitor screen revealed that
13 *PPP2R4*-depletion induced resistance against selumetinib (MEK inhibitor), but unexpectedly
14 sensitized cells for temsirolimus (mTOR inhibitor), *in vitro* and *in vivo*. Our findings
15 underscore a clinically relevant role for PTPA loss-of-function in *KRAS*-mutant NSCLC etiology
16 and kinase inhibitor response.

17

18 Keywords: *PPP2R4*, PP2A, *KRAS*, NSCLC, temsirolimus, selumetinib

19

20

21

22

23 **1. Introduction**

24 Non-small cell lung cancer (NSCLC) is the most common type of cancer worldwide and the
25 number one cause of cancer-related death (1). While the advent of targeted therapies has
26 benefited patients that harbor specific targetable driver mutations in EGFR and ALK genes,
27 they only represent a fraction of NSCLC patients. For *KRAS*-mutant NSCLC – which represents
28 the largest molecular subgroup of NSCLC – the clinical implementation of tailored therapies
29 has proven to be notoriously difficult and largely disappointing (2). Due to the hard to target
30 nature of *KRAS* itself, more easily targetable downstream kinase effectors in the
31 RAF/MEK/ERK and PI3K/AKT/mTOR pathways were long considered as suitable alternatives
32 (2, 3). However, most of the clinical trials focusing on downstream kinase inhibition have
33 proven to be unsuccessful, in part due to an incomplete understanding of mechanisms
34 determining therapy response and resistance (2, 3).

35 Although protein phosphatases, which counteract protein kinases, exhibit equally important
36 roles in determining net phosphorylation states of their substrates, their function in
37 tumorigenesis and therapy resistance only more recently started to gain attention. Members
38 of the multi-subunit Serine/Threonine Protein Phosphatase 2A (PP2A) family have a wide
39 range of functions in cellular and organismal homeostasis, and are considered to be major
40 tumor suppressors (4-6). PP2A exists mainly as trimeric holoenzymes, where a scaffolding A
41 subunit tethers the catalytic C subunit to any of a wide range of regulatory B subunits. The
42 identity of the incorporated B subunit determines substrate specificity, holoenzyme activity
43 and subcellular localization (4). Assembly and activation of PP2A as a trimeric holoenzyme is
44 a prerequisite for proper PP2A function and is a closely monitored process (7). Here, Protein
45 Phosphatase Two A Activator (PTPA), encoded by *PPP2R4*, plays a central role through
46 activation of the PP2A AC core dimer, which is followed by incorporation of the regulatory B
47 subunit (8-11).

48 Inactivation of PP2A is observed in many cancer types, both through genomic and non-
49 genomic mechanisms. Multiple PP2A subunits exhibit decreased expression, loss-of-function
50 mutations and deletions in a range of cancers (12-14). Moreover, overexpression of cellular
51 PP2A inhibitors CIP2A, SET or PME-1 are considered to be an important mechanism of non-
52 genomic PP2A inactivation, next to heterozygous loss of the PP2A activator PTPA (12-16).
53 For lung cancer specifically, recurrent mutations in the A α subunit gene *PPP2R1A* are found

54 at low frequency (17), while SET and CIP2A overexpression are commonly observed events,
55 associated with decreased lung cancer patient survival (18, 19).

56 PP2A acts on several points in the signaling pathways downstream of RAS, making it an
57 important regulator of RAS signaling output (6, 20), e.g. by direct dephosphorylation of AKT,
58 ERK1/2, mTOR, GSK-3 β and c-MYC, among others (4, 12-14). Notably, interference with
59 specific PP2A holoenzymes is a prerequisite for full-blown malignant conversion of
60 oncogenic RAS-dependent immortalized cells (21, 22). Moreover, inhibition of PP2A by
61 Okadaic Acid or genetic knockout promotes tumorigenesis in mice (16, 23-26), in part
62 associated with hyperactivation of downstream effectors of RAS (16, 25, 26). In addition,
63 knockin of a lung cancer-associated *PPP2R1A* mutation in *Kras*-mutant lung cancer mouse
64 models promotes tumorigenesis and decreases murine survival (27).

65 Importantly, PP2A inactivation was recently found to induce therapy resistance against a
66 wide range of targeted anti-cancer compounds, including MEK inhibition (28, 29). Moreover,
67 direct pharmacological activators of PP2A were identified as novel classes of promising anti-
68 cancer drugs in a broad range of cancers (28-35), including *KRAS*-mutant NSCLC (29). A
69 common denominator in several of these studies seemed to be the involvement of the
70 oncogenic transcription factor c-MYC (30), of which the stability is closely regulated by a
71 specific subset of PP2A holoenzymes (36-38).

72 Here, we specifically investigated the role of the PP2A activator PTPA in *KRAS*-mutant NSCLC
73 cancer etiology and therapeutic response. Our results identify PTPA as an important tumor
74 suppressor and modifier of targeted therapy outcomes in this hard-to-treat disease.

75 **2. Materials & Methods**

76 ***2.1 Cloning, site directed mutagenesis and recombinant His-PTPA production.***

77 Wild-type *PPP2R4* cDNA (isoform α ; (39)) was cloned into 3XFLAG-CMV10 (Sigma, E7658)
78 and pET15b (Sigma, 69661). *PPP2R4* FLAG-tag lentiviral expression vector (pLA CMV-N-Flag)
79 and *PPP2R4* 3'UTR targeting pLKO.1 (shPTPA) and control pLKO.1 (shGFP) were generated as
80 described in (22). PCR-based site-directed mutagenesis to generate PTPA point mutants was
81 performed with Pwo polymerase (Roche, 11644955001) and complementary DNA primers
82 (IDT DNA Technologies) containing the desired mutations (**Supplementary Table S1**).
83 Expression and purification of recombinant His-tagged PTPA was performed as described in
84 (16).

85 ***2.2 Cell culture, transfections and lentivirus production***

86 HEK293T (ATCC), A549 (Sigma, ECACC 86012805) and A427 (ATCC) cell lines were frozen at
87 early passage upon receipt and were routinely tested for *Mycoplasma* (Venor™ GeM,
88 Minerva Biolabs, 11-1050). Cell lines were cultured at 37°C/5% CO₂ in DMEM (Sigma, D6546)
89 (+ 10% fetal bovine serum (FBS; Sigma, F7524), 2 mM L-glutamine (Sigma, G7513) and
90 penicillin/streptomycin (100 units/mL and 10 mg/mL, respectively) (Sigma, P0781)).
91 Transfections were performed using polyethyleneimine (MW 25,000) (Polysciences Europe,
92 23966-2). Lentiviral infections were performed as described in The RNAi Consortium
93 Protocols
94 (<https://portals.broadinstitute.org/gpp/public/resources/protocols>).

95 ***2.3 Protein extraction, immunoprecipitation and western blotting***

96 Protein extraction and immunoprecipitation were performed as in (16), except that
97 NuPAGE™ 4-12%, Bis-Tris Midi Protein Gels (Invitrogen) were used for protein separation.
98 For FLAG-immunoprecipitations, ANTI-FLAG® M2 affinity gel (Sigma, A2220) was used.
99 Primary and secondary antibodies are indicated in **Supplementary Table S2**. Densitometric
100 analysis was performed using Image Studio™ Lite (LiCOR; RRID: SCR_013715).

101 ***2.4 Phosphorylase α PP2A reactivation assay***

102 The serine/threonine phosphatase activation by PTPA mutants was measured using P³²-
103 labeled phosphorylase α as a substrate for PP2A core dimer isolated from GST-PME-1
104 overexpressing HEK293T cells, as described in (16).

105 ***2.5 Anchorage-independent growth assays***

106 10,000 cells were seeded in triplicate in 0.35% Noble agar (Sigma, A5431) on top of a 0.5%
107 Noble agar base layer in 6-well plates (Greiner Bio-One, 65716) and fed twice weekly with
108 300 μ L complete DMEM. After 4 weeks, colonies were stained with 0.01% crystal violet in
109 20% methanol. 4x images were acquired at 5 standard coordinates and analyzed using
110 ImageJ (RRID:SCR_003070).

111 **2.6 Kinase inhibitor library screen and dose-response curves**

112 A549 shGFP and shPTPA cells were seeded in 96-well plates at a density of 2.000 cells/well
113 and treated for 72h. Cell viability was determined by Thiazolyl Blue Tetrazolium bromide
114 (MTT) (Alfa Aeser, L11939.06). Kinase inhibitors were selected based upon the known
115 regulation of their targets by PP2A and/or c-MYC, or regulation of PP2A and/or c-MYC by
116 their targets (**Supplementary Table 3A,3B**). Validations were performed in A427 cells, which
117 were seeded at 4000 cells/well. Dose-response curves were fitted using 3- or 4-parameter
118 logistic regression in GraphPad Prism 7.0 (GraphPad Software; RRID: SRC_002798).

119 **2.7 Animal experiments**

120 For xenografts, 10^6 cells were subcutaneously injected in the flanks of 5-6 week old female
121 Rj:NMRI-nu mice (Janvier). Tumor measurements started when tumors became palpable and
122 were performed at least twice weekly using a digital caliper. Volumes were calculated by
123 $length \times width^2 / 2$. Mice were sacrificed when tumors reached 2000 mm^3 , or in case of drug
124 treatments at treatment day 15. Drug treatments (**Supplementary Table 3A**) were initiated
125 at a mean tumor size of 150-300 mm^3 after randomization. For lung tumorigenesis, *Ppp2r4*
126 gene-trapped mice (16) were crossed with LSL-*KrasG12D* mice (40). At 6-12 weeks of age,
127 male and female *Ppp2r4*^{+/+};LSL-*KrasG12D*^{+/-}, *Ppp2r4*^{+/gt};LSL-*KrasG12D*^{+/-} and *Ppp2r4*^{gt/gt};LSL-
128 *KrasG12D*^{+/-} were intratracheally infected with $2,5 \times 10^7$ Cre-recombinase-encoding
129 adenoviral particles, as described in (41). 8 weeks weeks post-infection, anaesthetized mice
130 were exsanguinated and perfused with 0.9% NaCl. Lungs were dissected, fixated overnight at
131 4°C in 4% PFA and embedded in paraffin for sectioning (4 μ m thick) and H&E staining.
132 Images of 3 sections (100 μ m apart) were acquired (Axio Scan.Z1, Zeiss) at 20x magnification
133 and lesions were quantified in a blinded fashion using QuPath software (RRID: SCR_018257)
134 (42). All animal experiments were designed according to ARRIVE guidelines and approved by
135 the Animal Ethics Committee of the KU Leuven (project numbers P109/2013, P213/2017,
136 P087/2018).

137 **2.8 Immunohistochemical and immunofluorescence stainings**

138 Immunohistochemical (IHC) and immunofluorescence (IF) stainings of 4µm thick FFPE lung
139 sections and OCT preserved xenografts were performed with antibodies summarized in
140 **Supplementary Table 2** at indicated dilutions. For transgenic mice, proliferative index (PI)
141 was determined as number of Ki67+ CD45- cells, normalized to the number of nuclei (DAPI)
142 at 40X magnification of all observed lesions, in their entirety, for two *Ppp2r4^{+/+};LSL-*
143 *KrasG12D* and two *Ppp2r4^{+/-};LSL-KrasG12D* mice. For xenografts, Ki67 PI was determined as
144 number of positive nuclei normalized to the total number of detected nuclei per 20x
145 magnification fields of 3-6 random fields per tumor. Quantifications were performed using
146 QuPath software (RRID: SCR_018257).

147 **2.9 Cancer databases and survival analysis**

148 The Lung adenocarcinoma (TCGA, Firehose Legacy) study in cBioPortal (43, 44) was queried
149 for “PTPA: HOMLOSS; HETLOSS; MUT; CNA” and “KRAS”, “BRAF” or “EGFR”. Genomic and
150 clinical data were extracted for further stratification of patient groups based on *KRAS*, *BRAF*
151 or *EGFR* mutational status and *PPP2R4* genetic status or mRNA levels. The Catalog Of
152 Somatic Mutations In Cancer (COSMIC) was queried for “PPP2R4” and consulted for NSCLC-
153 associated *PPP2R4* somatic mutations. Kaplan-Meier survival analyses were performed with
154 GraphPad Prism 7.0 (Graphpad Software; RRID: SRC_002798).

155 **2.10 Statistics**

156 Statistical tests as indicated in the figure legends were performed using GraphPad Prism 7.0
157 (Graphpad Software; RRID: SRC_002798). *P*-values below 0.05 were considered significant.

158

159 **3. Results**

160 **3.1 *In vitro* recapitulation of PPP2R4 alterations underscores a clinical impact of PPP2R4**
 161 ***loss-of-function, specifically in KRAS-mutant NSCLC***

162 In the lung adenocarcinoma TCGA (Firehose Legacy) study, nearly half of the patients display
 163 heterozygous loss of *PPP2R4*, both in *KRAS* wild-type and mutant patient subsets (**Figure**
 164 **1A,1B**). Strikingly, for the *KRAS*-mutant NSCLC patient subset, we observed that *PPP2R4*
 165 heterozygous loss was associated with worse patient survival (**Figure 1C**). As *PPP2R4*
 166 genotype correlated with mRNA expression (**Figure 1A,1B**), the lower survival was also
 167 observed when stratifying on *PPP2R4* mRNA (**Figure 1D**). Notably, for *EGFR* and *BRAF*
 168 mutated patients, *PPP2R4* heterozygous loss rather showed a tendency to be associated
 169 with increased survival (**Suppl. Figure S1**).

170 Moreover, NSCLC studies included in the cBioPortal and COSMIC cancer databases revealed
 171 low frequency heterozygous *PPP2R4* point mutations, of which six – all in the most
 172 abundantly expressed α -isoform – were predicted to be detrimental for PTPA function
 173 (**Figure 1E**) (45). Indeed, while PTPA^{E225*} could not be detected at physiologically relevant
 174 levels (**Figure 1F**), binding to PP2A-C was diminished or abrogated for PTPA^{Y234C}, or PTPA^{H306L}
 175 and PTPA^{V316F}, respectively (**Figure 1F,1G**). Although PP2A-C binding was not affected for
 176 PTPA^{G240S} and even increased for PTPA^{R183L} (**Figure 1F,1G**), these mutants could not
 177 reactivate inactive PP2A-C to the same extent as PTPA^{WT}. PTPA^{R183L} did so to the same extent
 178 as the previously described PTPA^{G243V} mutant (16), while PTPA^{G240S} almost completely lacked
 179 PP2A-C reactivating potential (**Figure 1H, Figure S2A,S2B**).

180 To verify the survival disadvantage for the *KRAS*-mutant PTPA^{HETLOSS/low} patient subset, we
 181 stably knocked down PTPA in the *KRAS*-mutant (G12V) A549 lung cancer cell line (**Figure 1I**).
 182 This increased anchorage-independent growth as compared to shGFP-transduced control
 183 (**Figure 1J-1L**) and was rescued by re-introduction of PTPA^{WT}, but not by expression of PP2A-
 184 C non-binding PTPA^{V316F} (**Figure 1J-1L**). These findings underscore the relevance of NSCLC-
 185 associated *PPP2R4* dysfunctions in the ill-treatable *KRAS*-mutant NSCLC patient subset.

186

187 **3.2 *In vivo* reduction of PTPA expression aggravates KRAS-mutant NSCLC growth**

188 To provide *in vivo* evidence, shGFP and shPTPA A549 cells were subcutaneously injected into
 189 nude mice, and tumor growth was monitored. At endpoint, shPTPA A549 xenografted
 190 tumors were significantly larger and heavier as compared to shGFP control tumors (**Figure**

191 **2A-2C**). In line with our previous findings in spontaneous lymphomas of *Ppp2r4* gene
192 trapped mice (16), shPTPA A549 xenografts harvested at endpoint showed an
193 overexpression of the oncogenic transcription factor c-MYC (**Figure 2D-2G**), which could not
194 be attributed to changes in GSK-3 β S9 phosphorylation or ERK1/2 T202/Y204
195 phosphorylation (**Figure S3**).

196 In addition, we crossed *Ppp2r4* gene trapped mice (16) with a conditional LSL-*KrasG12D*
197 mouse model (40), yielding orthotopic lung adenocarcinoma development upon conditional
198 activation of the *KrasG12D*-allele by intratracheal instillation of Cre-encoding adenovirus
199 (41). We found a significantly increased number of early lung lesions (=atypical adenomatous
200 hyperplasia, AAH) in heterozygous as well as homozygous *Ppp2r4* gene trapped mice as
201 compared to wild-type at 8 weeks post tumor initiation (**Figure 3A,3B**). Moreover, we
202 observed a larger total size of lesions per lung area (**Figure 3C**), while the average lesion size
203 remained the same (**Figure 3D**). Similar TTF1 positivity across genotypes (data not shown)
204 indicated that loss of PTPA did not change the histology of mutant *KRAS*-driven lung
205 tumorigenesis. Importantly, Ki67 staining showed a higher proliferative index (PI) of the
206 lesions in PTPA-depleted mice (**Figure 3E**). Thus, we conclude that decreased PTPA
207 expression accelerated orthotopic mutant *KRAS*-driven lung tumor development *in vivo*.

208

209 **3.3 PTPA reduction affects the response of A549 cells on several kinase inhibitor therapies** 210 **acting downstream of KRAS**

211 PP2A dysfunction has recently been implicated in therapeutic resistance of endometrial and
212 lung cancer cells to kinase inhibition (28, 29). Together with the PTPA loss-associated
213 increase of c-MYC expression, another mediator of cancer therapy resistance (30), this
214 prompted us to assess the role of PTPA depletion on the therapeutic outcome of a range of
215 kinase inhibitor therapies. We assembled a confined library of 18 kinase inhibitors, of which
216 their targets are regulated by and/or regulate activity of either PP2A or c-MYC (**Supp. Table**
217 **3A,3B**). While most kinase inhibitor treatments remained equally potent (**Figure 4A,4B**), we
218 found that loss of PTPA led to increased resistance to selumetinib (MEK inhibition) or MK-
219 2206 (AKT inhibition) (**Figure 4A-4D**). On the other hand, temsirolimus (mTOR inhibition) and
220 barasertib (AURKB inhibition) both resulted in an increased growth inhibition of PTPA-
221 depleted cells as compared to wild-type (**Figure 4A,4B,4E,4F**).

222 While knockdown of PTPA increased c-MYC levels in xenografts (**Figure 2F,2G**), this appeared
223 not the case in basal 2D anchorage-dependent conditions (**Figure S4A**). Nevertheless,
224 shPTPA A549 cells were more resistant to reduction of c-MYC levels after treatment with
225 selumetinib, as compared to control cells (**Figure 4H,4L**). On the other hand, barasertib
226 reduced c-MYC levels more efficiently after PTPA knockdown (**Figure 4I,4M**). Treatment with
227 MK2206 or temsirolimus did not alter c-MYC levels regardless of PTPA expression (**Figure**
228 **4G,4J,4K,4N**). For each treatment, equal target inhibition was achieved in shGFP and shPTPA
229 A549s, as witnessed by P-ERK1/2 (selumetinib), P-HH3 (barasertib), GSK-3 β P-S9/total
230 (MK2206) and P-p70S6K (temsirolimus) (**Figure S4B-S4E**). Summarized, loss of PTPA induced
231 changes in therapeutic responses towards several kinase inhibitors *in vitro*, which for
232 selumetinib and barasertib correlated with changes at the level of c-MYC.

233 To validate the responses to the former four kinase inhibitors in a second human lung
234 adenocarcinoma cell line, dose-response curves were acquired in A427, another *KRAS*-
235 mutant cell line with much lower endogenous PTPA expression than A549 (**Figure 5A**). While
236 the responses to MK2206 or barasertib did not significantly differ between both cell lines
237 (**Figure 5C, 5E**), PTPA-low expressing A427 cells were more resistant to selumetinib (**Figure**
238 **5B**) and more sensitive to temsirolimus (**Figure 5D**) compared to PTPA-high expressing A549
239 cells, the latter two in line with the data from isogenic shGFP and shPTPA A549 cells.

240

241 **3.4 In vivo validation of kinase inhibition outcomes**

242 To further verify these findings in a biologically more relevant context, we treated mice
243 exhibiting shGFP and shPTPA A549 xenografts with selumetinib, MK2206, barasertib and
244 temsirolimus. While selumetinib and MK2206 were able to reduce growth both in shGFP and
245 shPTPA conditions, the growth of PTPA-depleted tumors was inhibited less dramatically as
246 compared to the shGFP controls at the endpoint of treatments (**Figure 6A, Figure S5A,S5C**),
247 confirming increased resistance to both compounds upon PTPA loss. Conversely, PTPA-
248 depleted xenografts were clearly more sensitive to temsirolimus treatment than shGFP
249 controls (**Figure 6B, Figure S5B**). On the other hand, barasertib treatments did not
250 significantly differ between shPTPA and shGFP tumors at endpoint (**Figure S5D**). Importantly,
251 Ki67-based proliferation index was significantly higher in the untreated shPTPA xenografts as
252 compared to shGFP controls (**Figure 6C-6F, Figure S5E,S5F**), remained higher in the

253 selumetinib- or MK2206-treated groups (**Figure 6C,6E, Figure S5E,S5F**), but was no longer
254 significantly different between the temsirolimus-treated groups (**Figure 6D,6F**).

255 To further underscore these findings, we analyzed our data by adapted RECIST criteria,
256 which use 'change from baseline' as parameters to determine 'outcome' (= 'partial
257 response', 'stable disease', 'progressive disease'). Once again, our findings clearly point
258 towards the more refractory behavior of shPTPA tumors as compared to shGFP when
259 treated with MK2206 or selumetinib (**Figure S6A,S6C**), and to the higher sensitivity of
260 shPTPA tumors, when treated with temsirolimus (**Figure S6B,S6D**).

261 In summary, we demonstrated for at least two kinase inhibitors that the results from long-
262 term in vivo xenograft growth assays are consistent with short-term cell viability results in
263 two independent *KRAS*-mutant cell lines: PTPA-depletion or low PTPA expression clearly
264 resulting in increased resistance for selumetinib, while increasing sensitivity for
265 temsirolimus.

266

267 ***3.5. Loss-of-PTPA-associated responses to selumetinib correlate with changes in c-MYC***
268 ***expression, while loss-of-PTPA-associated responses to temsirolimus correlate with***
269 ***increased dephosphorylation of p70 S6 kinase***

270 Selumetinib treatment resulted in nearly undetectable phospho-ERK1/2 levels in both shGFP
271 and shPTPA A549 xenografts (**Figure 7A,7B**), while c-MYC expression, although decreased
272 upon treatment in both groups, still remained higher in the shPTPA tumors compared to the
273 shGFP group (**Figure 7C,7D**) – providing a potential mechanism of selumetinib resistance
274 (29).

275 Although there was no significant difference in basal phospho-p70 S6K levels in shGFP versus
276 shPTPA A549 xenografts (**Figure 8A,8B**), temsirolimus treatment resulted in significantly
277 lower p70 S6 kinase phosphorylation levels in shPTPA as opposed to shGFP xenografts
278 (**Figure 8A,8B**). With p70 S6 kinase as a major mTOR target, this provides a potential
279 mechanism for the increased sensitivity for temsirolimus upon loss of PTPA.

280

281 **4. Discussion**

282 *KRAS*-mutant lung adenocarcinomas represent the largest subgroup of non-small cell lung
283 cancer (NSCLC), the most common and deadly cancer worldwide (1, 2). As no targeted
284 therapy tailored on *KRAS* driver mutation status has been clinically approved so far,

285 understanding mechanisms of therapy resistance against inhibition of oncogenic kinases
286 downstream of *KRAS* remains important (2, 3). We focused on a role for the Protein
287 Phosphatase 2A (PP2A) Activator PTPA in *KRAS*-mutant NSCLC, due to the implication of
288 PP2A in the regulation of oncogenic kinases downstream of RAS (4, 12, 13), PP2A
289 inactivation in a broad range of cancers (12, 13), and the emerging role for PP2A inactivation
290 as an important mechanism of cancer therapy resistance (28, 29).

291 Across COSMIC and cBioPortal lung adenocarcinoma studies, we retrieved a low number of
292 PTPA point mutations. All PTPA α isoform mutants were found to be defective, either
293 through loss of binding to the PP2A catalytic subunit, or through attenuation of PP2A
294 reactivating potential. These findings are in line with their localization in the proximity of
295 functionally important domains, based on structure-function and crystallographic studies of
296 PTPA (9, 11). More importantly, in the lung adenocarcinoma (TCGA, Firehose Legacy) study,
297 we observed a wide distribution of *PPP2R4* mRNA, which was directly proportional to loss or
298 gain of its gene locus. Heterozygous loss (44% of patients) of *PPP2R4* and low *PPP2R4* mRNA
299 was significantly associated with worse survival in *KRAS*-mutant patients, but not in *EGFR*- or
300 *BRAF*-mutant patients. This further expands the overall number of cancer types where PTPA
301 status impacts patient survival (16). PTPA dysfunction thus joins other clinically-relevant
302 PP2A inactivating mechanisms previously described in lung cancer, such as overexpression of
303 the cellular PP2A inhibitors CIP2A (18) and SET (19), and low-frequency inactivating
304 mutations in the α subunit gene *PPP2R1A* (17).

305 Mimicking the clinically observed loss of PTPA by shRNA-mediated knockdown increased
306 anchorage-independent and xenograft growth of *KRAS*-mutant A549 lung adenocarcinoma,
307 and was associated with a higher proliferation index (Ki67 expression). Moreover, the
308 increased number of early lung lesions (atypical adenomatous hyperplasia), the larger total
309 size of lesions per lung area and the higher proliferation index of lesions observed in
310 *Ppp2r4*^{+/*gt*};LSL-*Kras*G12D and *Ppp2r4*^{gt/*gt*};LSL-*Kras*G12D mice as compared to *Ppp2r4*^{+/*+*};LSL-
311 *Kras*G12D mice further supported the role of PTPA as a tumor suppressor in *KRAS*-mutant
312 NSCLC. In xenografts, PTPA reduction resulted in overexpression of c-MYC, a transcription
313 factor deregulated in a multitude of cancers, and an important facilitator of RAS-driven
314 tumorigenesis (36, 46). This is in line with findings from the RAS-driven HEK-TER system,
315 where loss of PTPA induced full transformation of immortalized HEK-TER cells, associated
316 with overexpression of c-MYC (22). Moreover, we previously observed c-MYC

317 overexpression in spontaneous lymphomas of *Ppp2r4* gene trapped mice (16). As loss of
318 PTPA induces a selective reduction of PP2A-B' holoenzymes (16), we speculate the increase
319 in c-MYC levels might at least in part be attributed through loss of B'α containing
320 holoenzymes that are known to destabilize c-MYC through dephosphorylation of Serine-62
321 (37). Unfortunately, however, we could not solidly prove this hypothesis, due to suboptimal
322 quality of commercially available phospho-c-MYC antibodies in our hands. In any case, the
323 lack of significant changes in P-ERK1/2 and GSK-3β activity (two upstream c-MYC kinases)
324 rules out their involvement in increasing c-MYC after PTPA knockdown.

325 MYC overexpression is a well-known mediator of therapy resistance (30), and recent
326 publications have identified PP2A dysfunction as a new partner in crime (28, 29). We have
327 now identified kinase inhibitors of which the efficiency is influenced by decreased PTPA
328 expression in *KRAS*-mutant cells. While selumetinib and MK2206 proved to be less efficient
329 to suppress growth after PTPA knockdown, temsirolimus and barasertib did so to a better
330 extent in our initial A549 screen. However, subsequent *in vivo* validation experiments only
331 confirmed the altered responses of shPTPA cells for selumetinib, MK2206 and temsirolimus.
332 A second, short-term validation experiment in another *KRAS*-mutant lung adenocarcinoma
333 cell line further confirmed the higher resistance of PTPA-low expressing A427 cells for
334 selumetinib, as well as the increased sensitivity for temsirolimus, when compared with
335 PTPA-high expressing A549 cells. Mechanistically, we found a correlation between
336 maintained higher c-MYC expression levels in shPTPA cells upon selumetinib treatment *in*
337 *vitro* (**Figure 4H,4L**) and *in vivo* (**Figure 7B,7D**), an observation which had previously been
338 reported in the same cell line (A549) as the causal mechanism of increased resistance to
339 MEK inhibitors upon PP2A inhibition by siRNA-mediated knockdown of the Aα subunit (29).
340 Thus, we deem it very likely that PP2A inhibition upon knockdown of PTPA may mediate
341 MEK inhibitor resistance by the same mechanism. In contrast, the increased sensitivity of
342 PTPA-depleted cells for mTOR inhibitors seemed independent of any alterations in c-MYC
343 expression (**Figure 4J,4N**), but instead could be correlated to a stronger decrease in
344 phospho-p70 S6 kinase (**Figure 8A,8B**). Exactly how the specific PP2A dysfunction(s) caused
345 by decreased PTPA expression would contribute to these observations, remains to be further
346 determined.

347 Altogether, our findings underscore that heterozygous loss of PTPA, as a novel mechanism of
348 PP2A dysfunction in *KRAS*-mutant NSCLC, contributes to increased malignancy and altered

349 therapeutic outcomes upon use of kinase inhibitors. Most significantly, while PTPA depletion
 350 in *KRAS*-mutant NSCLC causes resistance to the MEK inhibitor selumetinib, it creates an
 351 unexpected window of treatment opportunity for the mTOR inhibitor temsirolimus. These
 352 findings could become of clinical importance upon implementation of the *PPP2R4* status as
 353 an additional stratification marker in *KRAS*-mutant NSCLC.

354

355 **5. Acknowledgments**

356 We would like to thank Prof. Mariano Barbacid, Prof. David Santamaria and Dr. Patricia Nieto
 357 (CNIO, Madrid, Spain) for their hospitality and educating BM in the technique of
 358 intratracheal instillation of mice with Ad-Cre virus. Prof. Johan Van Lint (KU Leuven, Belgium)
 359 and Prof. Rita Derua (KU Leuven, Belgium) are acknowledged for their continuous support.
 360 Lab members and Dr. Mathias Cobbaut (Francis Crick Institute, London, UK) are
 361 acknowledged for valuable discussions and critical reading of the manuscript. Prof. Chris
 362 Marine (VIB-KUL) is acknowledged for kindly sharing the LSL-*Kras*G12D mouse model. BM
 363 was supported by a fellowship from the KU Leuven Research Council (BOF DB/15/011/BM).
 364 JDO received an FWO-SB fellowship from the Research Foundation-Flanders. JJV and VJ were
 365 jointly funded by the Belgian Foundation Against Cancer (FAC-F/2016/822). AS and VJ were
 366 jointly funded by a KU Leuven C2-project (C24/17/073). VJ was additionally supported by the
 367 Research Foundation-Flanders (G.OB01.16N).

368

369 **6. References**

- 370 1. F. Bray *et al.*, Global cancer statistics 2018: GLOBOCAN estimates of incidence and
 371 mortality worldwide for 36 cancers in 185 countries. *CA Cancer J Clin* **68**, 394-424
 372 (2018).
- 373 2. I. Ferrer *et al.*, *KRAS*-Mutant non-small cell lung cancer: From biology to therapy.
 374 *Lung Cancer* **124**, 53-64 (2018).
- 375 3. M. Drosten, M. Barbacid, Targeting the MAPK Pathway in *KRAS*-Driven Tumors.
 376 *Cancer Cell* **37**, 543-550 (2020).
- 377 4. V. Janssens, J. Goris, Protein phosphatase 2A: a highly regulated family of
 378 serine/threonine phosphatases implicated in cell growth and signalling. *Biochem J*
 379 **353**, 417-439 (2001).
- 380 5. S. Reynhout, V. Janssens, Physiologic functions of PP2A: Lessons from genetically
 381 modified mice. *Biochim Biophys Acta Mol Cell Res* **1866**, 31-50 (2019).
- 382 6. M. Mumby, PP2A: unveiling a reluctant tumor suppressor. *Cell* **130**, 21-24 (2007).
- 383 7. W. Sents, E. Ivanova, C. Lambrecht, D. Haesen, V. Janssens, The biogenesis of active
 384 protein phosphatase 2A holoenzymes: a tightly regulated process creating phosphatase
 385 specificity. *FEBS J* **280**, 644-661 (2013).

- 386 8. T. Fellner *et al.*, A novel and essential mechanism determining specificity and activity
387 of protein phosphatase 2A (PP2A) in vivo. *Genes Dev* **17**, 2138-2150 (2003).
- 388 9. N. Leulliot *et al.*, Crystal structure of the PP2A phosphatase activator: implications for
389 its PP2A-specific PPIase activity. *Mol Cell* **23**, 413-424 (2006).
- 390 10. H. Hombauer *et al.*, Generation of active protein phosphatase 2A is coupled to
391 holoenzyme assembly. *PLoS Biol* **5**, e155 (2007).
- 392 11. F. Guo *et al.*, Structural basis of PP2A activation by PTPA, an ATP-dependent
393 activation chaperone. *Cell Res* **24**, 190-203 (2014).
- 394 12. P. J. Eichhorn, M. P. Creighton, R. Bernards, Protein phosphatase 2A regulatory
395 subunits and cancer. *Biochim Biophys Acta* **1795**, 1-15 (2009).
- 396 13. B. Meeusen, V. Janssens, Tumor suppressive protein phosphatases in human cancer:
397 Emerging targets for therapeutic intervention and tumor stratification. *Int J Biochem*
398 *Cell Biol* **96**, 98-134 (2018).
- 399 14. D. Perrotti, P. Neviani, Protein phosphatase 2A: a target for anticancer therapy. *Lancet*
400 *Oncol* **14**, e229-238 (2013).
- 401 15. O. Kauko, J. Westermarck, Non-genomic mechanisms of protein phosphatase 2A
402 (PP2A) regulation in cancer. *Int J Biochem Cell Biol* **96**, 157-164 (2018).
- 403 16. W. Sents *et al.*, PP2A Inactivation Mediated by *PPP2R4* haploinsufficiency promotes
404 cancer development. *Cancer Res* **77**, 6825-6837 (2017).
- 405 17. G. A. Calin *et al.*, Low frequency of alterations of the alpha (PPP2R1A) and beta
406 (PPP2R1B) isoforms of the subunit A of the serine-threonine phosphatase 2A in
407 human neoplasms. *Oncogene* **19**, 1191-1195 (2000).
- 408 18. Q. Z. Dong *et al.*, CIP2A is overexpressed in non-small cell lung cancer and correlates
409 with poor prognosis. *Ann Surg Oncol* **18**, 857-865 (2011).
- 410 19. H. Liu *et al.*, Overexpression of PP2A inhibitor SET oncoprotein is associated with
411 tumor progression and poor prognosis in human non-small cell lung cancer.
412 *Oncotarget* **6**, 14913-14925 (2015).
- 413 20. J. Westermarck, W. C. Hahn, Multiple pathways regulated by the tumor suppressor
414 PP2A in transformation. *Trends Mol Med* **14**, 152-160 (2008).
- 415 21. W. Chen *et al.*, Identification of specific PP2A complexes involved in human cell
416 transformation. *Cancer Cell* **5**, 127-136 (2004).
- 417 22. A. A. Sablina, M. Hector, N. Colpaert, W. C. Hahn, Identification of PP2A complexes
418 and pathways involved in cell transformation. *Cancer Res* **70**, 10474-10484 (2010).
- 419 23. H. Fujiki *et al.*, Mechanisms of action of okadaic acid class tumor promoters on
420 mouse skin. *Environ Health Perspect* **93**, 211-214 (1991).
- 421 24. G. Walter, R. Ruediger, Mouse model for probing tumor suppressor activity of protein
422 phosphatase 2A in diverse signaling pathways. *Cell Cycle* **11**, 451-459 (2012).
- 423 25. M. Janghorban *et al.*, The tumor suppressor phosphatase PP2A-B56 α regulates
424 stemness and promotes the initiation of malignancies in a novel murine model. *PLoS*
425 *One* **12**, e0188910 (2017).
- 426 26. C. Lambrecht *et al.*, Loss of protein phosphatase 2A regulatory subunit B56 δ
427 promotes spontaneous tumorigenesis in vivo. *Oncogene* **37**, 544-552 (2018).
- 428 27. R. Ruediger, J. Ruiz, G. Walter, Human cancer-associated mutations in the A α subunit
429 of protein phosphatase 2A increase lung cancer incidence in A α knock-in and
430 knockout mice. *Mol Cell Biol* **31**, 3832-3844 (2011).
- 431 28. C. M. O'Connor *et al.*, Inactivation of PP2A by a recurrent mutation drives resistance
432 to MEK inhibitors. *Oncogene* **39**, 703-717 (2020).
- 433 29. O. Kauko *et al.*, PP2A inhibition is a druggable MEK inhibitor resistance mechanism
434 in KRAS-mutant lung cancer cells. *Sci Transl Med* **10**, (2018).

- 435 30. C. C. Farrington *et al.*, Protein phosphatase 2A activation as a therapeutic strategy for
436 managing MYC-driven cancers. *J Biol Chem* **295**, 757-770 (2020).
- 437 31. J. Sangodkar *et al.*, Activation of tumor suppressor protein PP2A inhibits KRAS-
438 driven tumor growth. *J Clin Invest* **127**, 2081-2090 (2017).
- 439 32. G. L. Coles *et al.*, Unbiased Proteomic Profiling Uncovers a Targetable
440 GNAS/PKA/PP2A Axis in Small Cell Lung Cancer Stem Cells. *Cancer Cell* **38**, 129-
441 143.e127 (2020).
- 442 33. S. E. Taylor *et al.*, The Highly Recurrent PP2A A α -Subunit Mutation P179R Alters
443 Protein Structure and Impairs PP2A Enzyme Function to Promote Endometrial
444 Tumorigenesis. *Cancer Res* **79**, 4242-4257 (2019).
- 445 34. P. Neviani *et al.*, PP2A-activating drugs selectively eradicate TKI-resistant chronic
446 myeloid leukemic stem cells. *J Clin Invest* **123**, 4144-4157 (2013).
- 447 35. K. Morita *et al.*, Allosteric Activators of Protein Phosphatase 2A Display Broad
448 Antitumor Activity Mediated by Dephosphorylation of MYBL2. *Cell* **181**, 702-
449 715.e720 (2020).
- 450 36. E. Yeh *et al.*, A signalling pathway controlling c-Myc degradation that impacts
451 oncogenic transformation of human cells. *Nat Cell Biol* **6**, 308-318 (2004).
- 452 37. H. K. Arnold, R. C. Sears, Protein phosphatase 2A regulatory subunit B56alpha
453 associates with c-myc and negatively regulates c-myc accumulation. *Mol Cell Biol* **26**,
454 2832-2844 (2006).
- 455 38. L. Zhang *et al.*, Eya3 partners with PP2A to induce c-Myc stabilization and tumor
456 progression. *Nat Commun* **9**, 1047 (2018).
- 457 39. V. Janssens *et al.*, Identification and characterization of alternative splice products
458 encoded by the human phosphotyrosyl phosphatase activator gene. *Eur J Biochem*
459 **267**, 4406-4413 (2000).
- 460 40. E. L. Jackson *et al.*, Analysis of lung tumor initiation and progression using
461 conditional expression of oncogenic K-ras. *Genes Dev* **15**, 3243-3248 (2001).
- 462 41. M. DuPage, A. L. Dooley, T. Jacks, Conditional mouse lung cancer models using
463 adenoviral or lentiviral delivery of Cre recombinase. *Nat Protoc* **4**, 1064-1072 (2009).
- 464 42. P. Bankhead *et al.*, QuPath: Open source software for digital pathology image
465 analysis. *Sci Rep* **7**, 16878 (2017).
- 466 43. E. Cerami *et al.*, The cBio cancer genomics portal: an open platform for exploring
467 multidimensional cancer genomics data. *Cancer Discov* **2**, 401-404 (2012).
- 468 44. J. Gao *et al.*, Integrative analysis of complex cancer genomics and clinical profiles
469 using the cBioPortal. *Sci Signal* **6**, p11 (2013).
- 470 45. Y. Choi, G. E. Sims, S. Murphy, J. R. Miller, A. P. Chan, Predicting the functional
471 effect of amino acid substitutions and indels. *PLoS One* **7**, e46688 (2012).
- 472 46. P. Hydbring *et al.*, Phosphorylation by Cdk2 is required for Myc to repress Ras-
473 induced senescence in cotransformation. *Proc Natl Acad Sci U S A* **107**, 58-63 (2010).
- 474 47. R. Sears *et al.*, Multiple Ras-dependent phosphorylation pathways regulate Myc
475 protein stability. *Genes Dev* **14**, 2501-2514 (2000).
- 476 48. J. Jiang *et al.*, Direct Phosphorylation and Stabilization of MYC by Aurora B Kinase
477 Promote T-cell Leukemogenesis. *Cancer Cell* **37**, 200-215.e205 (2020).
- 478 49. M. J. West, M. Stoneley, A. E. Willis, Translational induction of the c-myc oncogene
479 via activation of the FRAP/TOR signalling pathway. *Oncogene* **17**, 769-780 (1998).
- 480
481
482
483
484

485
486
487
488
489
490
491
492
493
494
495
496
497
498
499
500
501
502
503
504
505
506
507
508
509
510
511
512
513
514
515
516
517
518

7. Figure legends

Figure 1: *PPP2R4*, the gene encoding the protein phosphatase 2A activator PTPA, displays non-conservative point mutations and clinically relevant heterozygous loss in non-small cell lung adenocarcinoma, particularly in the *KRAS*-mutant subgroup.

A,B: Distribution of *PPP2R4* mRNA expression across *PPP2R4* genotypes in complete Lung adenocarcinoma (TCGA, Firehose Legacy) cohort (A) and *KRAS*-mutant subcohort (B). Data are represented as mean +/- SD. Statistics: One-way ANOVA. *: $p < 0.05$; ***: $p < 0.0001$; ****: $p < 0.0001$. **C,D:** Kaplan-Meier analysis of *KRAS*-mutant patients in the lung adenocarcinoma TCGA (provisional study) stratified according to their *PPP2R4* genotype (C) and *PPP2R4* mRNA expression (50 highest vs. 50 % lowest) (D). Statistics: Log-rank test. *: $p < 0.05$. **E:** Lung adenocarcinoma-associated PTPA isoform α variants are predicted to be loss-of-function. Numbers indicate amino acid position of the mutations based on the longest human PTPA isoform (β). D92 is unique to PTPA isoform β . **F:** Assessment of PP2A-C binding of PTPA mutants by immunoprecipitation and Western blotting. Lysates of FLAG-PTPA wild-type and mutant overexpressing HEK293T were FLAG-immunoprecipitated, and IPs were counterstained for endogenous PP2A-C subunit. **G:** Quantifications of panel F. Statistics: One-way ANOVA. *: $p < 0.05$; **: $p < 0.01$; ***: $p < 0.001$; ****: $p < 0.0001$. **H:** PME1-bound PP2A reactivation capacities of PTPA mutants as compared to wild-type PTPA. Activities are expressed as relative CPM (counts per minute) values compared to PTPA wild-type at 5 minutes (=100%). N=3. Statistics: Two-way ANOVA. *: $p < 0.05$; **: $p < 0.001$; ****: $p < 0.0001$. **I:** PTPA knockdown in the *KRAS*-mutant A549 non-small cell lung cancer cell line and rescue with FLAG-tagged wild-type and mutant PTPA. VINC: Vinculin. **J:** Representative images of anchorage-independent growth of stable A549 cell lines in soft agar. **K,L:** Quantifications of colony number (K) and area (L). Statistics: One-way ANOVA. ***: $p < 0.001$, as compared to shGFP_EV.

519 **Figure 2: Xenograft mouse models further corroborate evidence for PTPA as a tumor**
 520 **suppressor in *KRAS*-mutant lung adenocarcinoma**

521 **A:** Images of A549 shGFP and shPTPA xenografted tumors at endpoint. Weights and volumes
 522 are indicated per individual tumor. **B:** Tumor weights (mg) at endpoint. Statistics: Two-sided
 523 student's t-test. *: $p < 0.05$. **C:** Tumor volumes (mm^3) over time. Statistics: Two-way ANOVA.
 524 *: $p < 0.05$. Western blots (**D,F**) and quantifications (**E,G**) of A549 shGFP versus A549 shPTPA
 525 xenografts. VINC: Vinculin. Statistics: Two-sided student's t-test. **: $p < 0.01$.

526
 527 **Figure 3: Loss of *Ppp2r4* in a *LSL-KrasG12D;Ptpa*-genetrap transgenic mouse model induces**
 528 **lung tumor initiation.**

529 **A:** Representative images of H&E stainings displaying *Kras*(G12D)-induced lung tumorigenesis
 530 in *Ppp2r4*^{+/+} (=WT), *Ppp2r4*^{+/*gt*} (=HE) and *Ppp2r4*^{*gt/gt*} (=HO) mice. **B:** Mean number of lesions
 531 per lung section. **C:** Quantification of atypical adenomatous hyperplasia (AAH) and total size
 532 relative to the lung area in *Ppp2r4*^{+/+} (= WT), *Ppp2r4*^{+/*gt*} (=HE) and *Ppp2r4*^{*gt/gt*} (=HO) mice, 8
 533 weeks post AdCre infection. **D:** Mean size of AAH lesions. **E:** Proliferative index Ki67 staining
 534 of two *Ppp2r4* wild-type (WT) and two *Ppp2r4* heterozygous (HE) *LSL-KrasG12D* mice, 8
 535 weeks post AdCre infection. **Statistics:** One-way ANOVA. **: $p < 0.01$; ***: $p < 0.001$. WT: wild-
 536 type; HE: heterozygotes; HO: homozygotes.

537
 538 **Figure 4: A confined kinase inhibitor screen reveals PTPA loss-induced changes in growth**
 539 **response of A549 cells towards different targeted kinase inhibitors.**

540 **A, B:** Fold-changes (shPTPA/shGFP) in EC50s for 18 kinase inhibitors, as measured by MTT
 541 after 72 hours of treatment. Compounds to which loss of PTPA induced resistance are
 542 depicted in red, while compounds with improved responses are depicted in green. Each
 543 point represents a biological replicate (**A**). Significance levels were determined using ratio-
 544 paired t-tests (**A,B**), and are represented as $-\log_{10}(\text{p-value})$ in (**B**). **C-F:** Representative dose-
 545 response curves of significantly affected compounds. EC50s and p -values were determined
 546 by 4-parameter non-linear regression. **G-J:** Representative Western blot analyses of c-MYC
 547 responses of cells treated at indicated doses for 48 hours. **K-N:** Quantifications of c-MYC
 548 levels 48 hours after treatment at indicated doses of at least 3 biological replicates.
 549 Statistics: One-way ANOVA. **: $p < 0.01$.

550

551 **Figure 5: Low PTPA expression is associated with differential response towards**
 552 **selumetinib and temsirolimus for A427 and A529 KRAS-mutant NSCLC cell lines.**

553 **A:** Western blots of cell lysates of A427 and A549 cells, developed with the indicated
 554 antibodies. **B:** Dose-response curves of selumetinib: $EC_{50_{A549}} = 24.56$ nM vs. $EC_{50_{A427}} = 265.9$
 555 nM ($p < 0.0001$). **C:** Dose-response curves of MK2206 (n.s.). **D:** Dose-response curves for
 556 temsirolimus: $EC_{50_{A549}} = 1.260$ nM vs. $EC_{50_{A427}} = 0.1410$ nM ($p = 0.0002$). **E:** Dose-resposne
 557 curves of barasertib (n.s.). Error bars represent mean +/- SEM.

558

559 **Figure 6: *In vivo* treatment outcomes of A549 xenografts against selumetinib and**
 560 **temsirolimus are affected by loss of PTPA.**

561 **A,B:** Growth increment (% as of baseline volume) represented across treatment duration,
 562 which was initiated at mean tumor volumes between 150 mm^3 and 300 mm^3 . Selumetinib
 563 and and temsirolimus treatment cohorts were compared to independent shGFP and shPTPA
 564 vehicle control groups. Selumetinib was administered at 25 mg/kg daily, for 15 days
 565 continuously. Temsirolimus was administered at 5 mg/kg for 16 days (intermittent dosing
 566 schedule). Statistics: Two-way ANOVA. *: $p < 0.05$; ***: $p < 0.001$; ****: $p < 0.0001$. Data are
 567 shown as mean +/- SEM. **C,D:** Quantifications of Ki67 proliferative index across in
 568 selumetinib (**C**) and temsirolimus (**D**) treated and control shGFP and shPTPA xenografts.
 569 Statistics: One-way ANOVA. *: $p < 0.05$; **: $p < 0.01$; ***: $p < 0.001$; ^: border-line significance
 570 ($p = 0.09$). **E,F:** Representative images of Ki67-stainings of xenografts from the indicated
 571 genotypes, and treated with indicated kinase inhibitors. Scale bars represent $100 \mu\text{m}$.

572

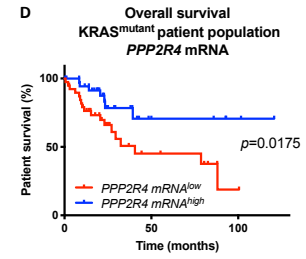
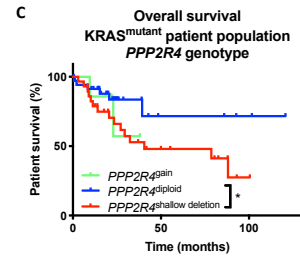
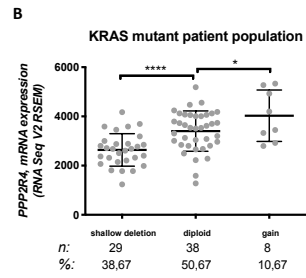
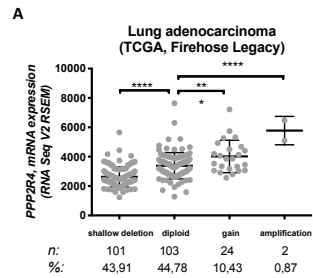
573 **Figure 7: Loss of PTPA is associated with changes in c-MYC expression upon selumetinib**
 574 **treatment *in vivo*.**

575 **A, C:** Western blot analysis of P-ERK and c-MYC after treatment with selumetinib at day 15 of
 576 treatment (25mk/kg). **B,D:** Quantifications of P-ERK1/2 levels (**B**) and total c-MYC levels (**D**)
 577 normalized to vinculin. Data are shown as mean +/- SEM. Statistics: One-way ANOVA. *:
 578 $p < 0.05$; **: $p < 0.01$; ***: $p < 0.001$; ****: $p < 0.0001$. VINC: vinculin.

579

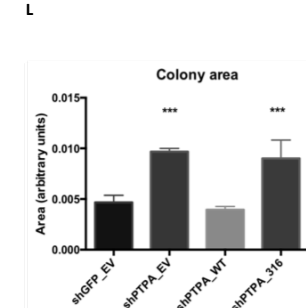
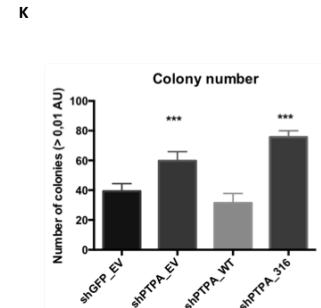
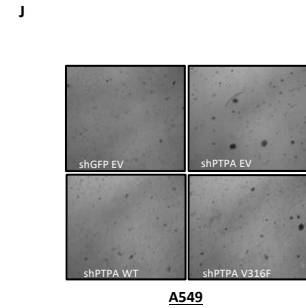
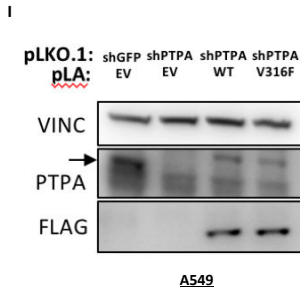
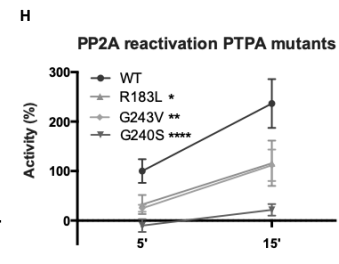
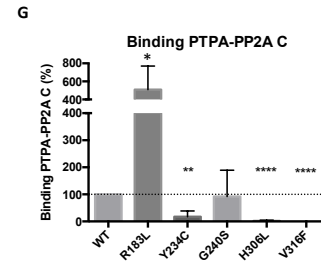
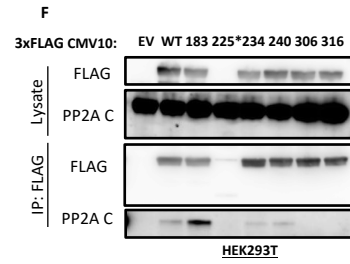
580 **Figure 8: Sensitivity towards temsirolimus upon loss of PTPA can be traced back to**
 581 **differential mTOR signaling.**

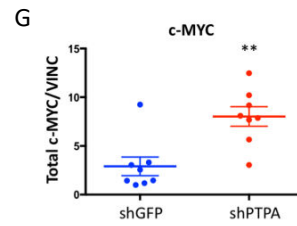
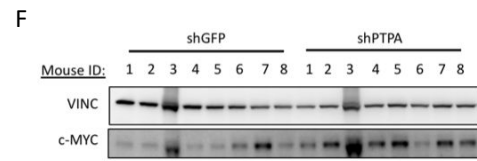
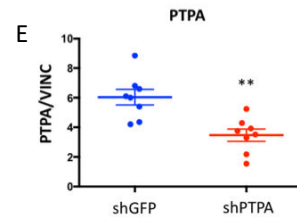
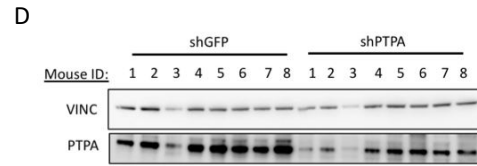
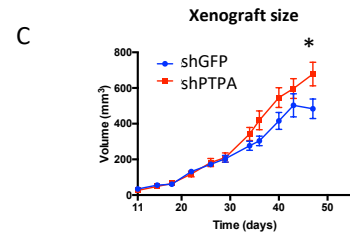
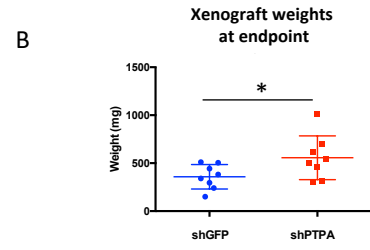
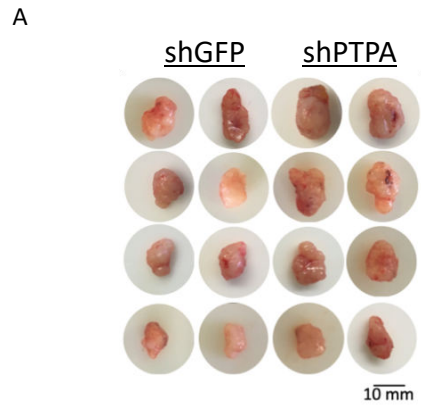
582 **A:** Western blot analysis of p70S6K and P-p70S6K at day 16 of temsirolimus treatment
583 (5mk/kg). VINC: vinculin. **B-D:** Quantifications of P-p70S6K levels (**B**), total p70S6K (**C**), and
584 phospho/total p70S6K, normalized to vinculin. Data are shown as mean +/- SEM. Statistics:
585 One-way ANOVA. *: $p < 0.05$; **: $p < 0.01$; ~: $p = 0.07$ (**C**) and 0.13 (**D**).
586



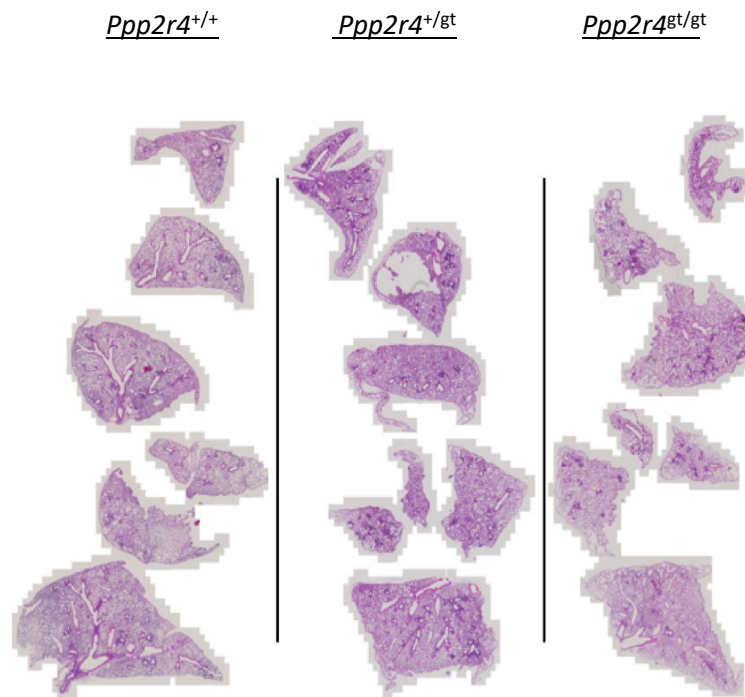
E

AA substitution	PROVEAN score	prediction (cut-off = -2.5)
D92N	-0.17	Neutral
R183L	-6.63	Deleterious
E225*	-481.09	Deleterious
Y234C	-8.75	Deleterious
G240S	-5.83	Deleterious
H306L	-10.11	Deleterious
V316F	-4.73	Deleterious

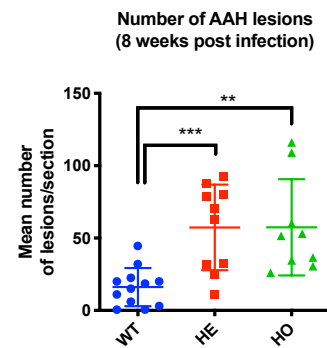




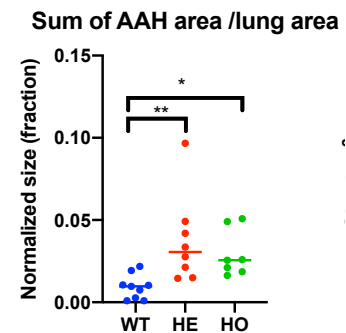
A



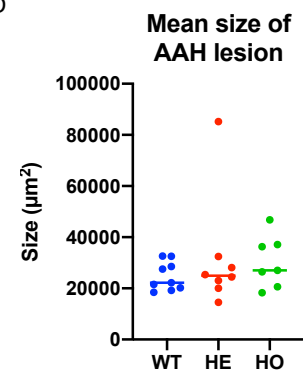
B



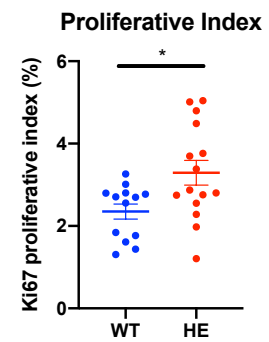
C

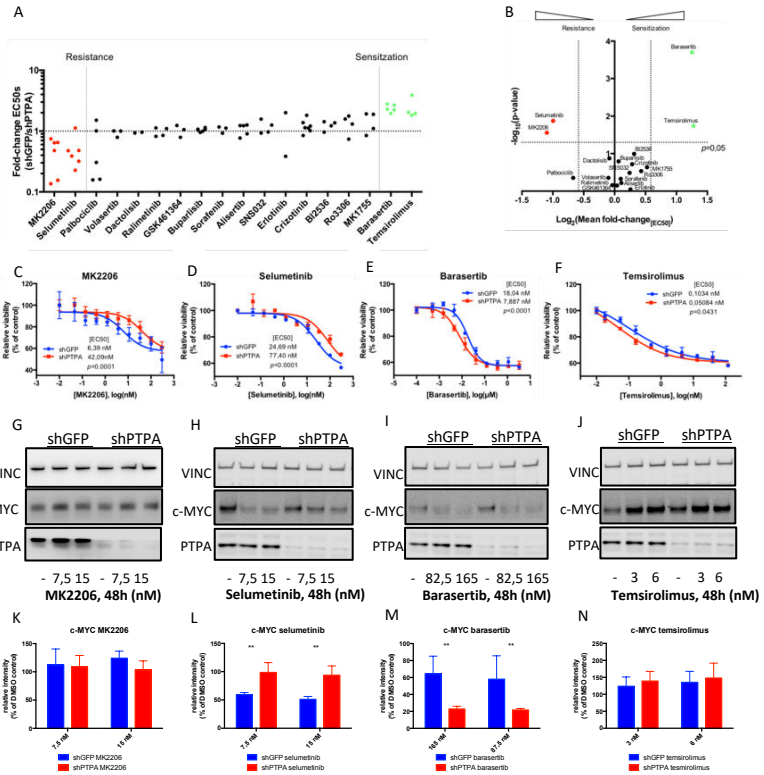


D

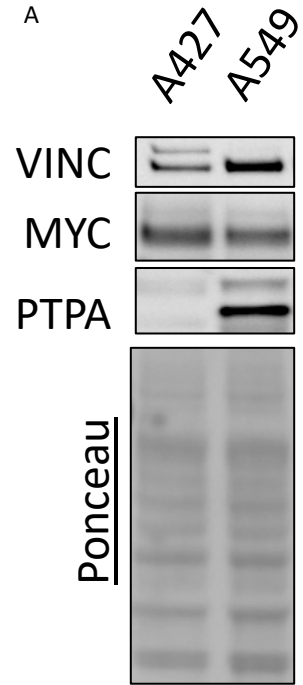


E

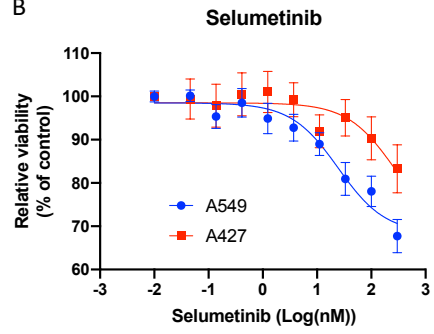




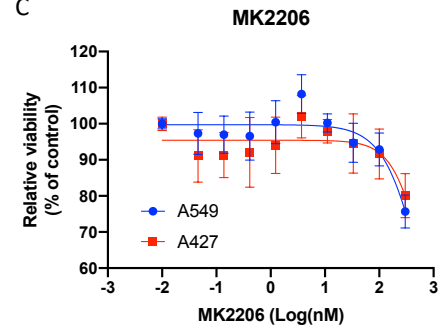
A



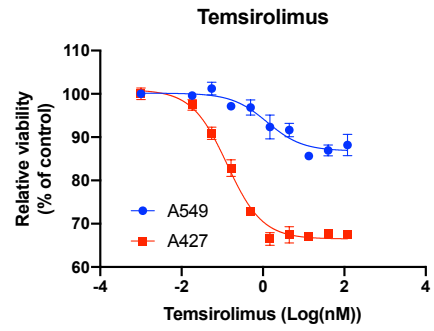
B



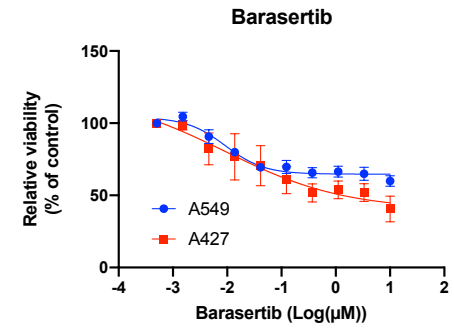
C

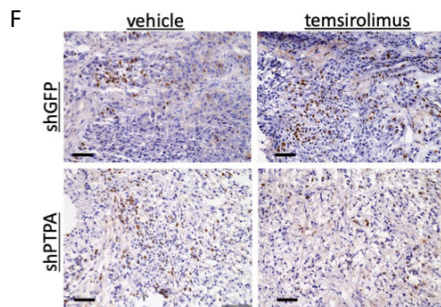
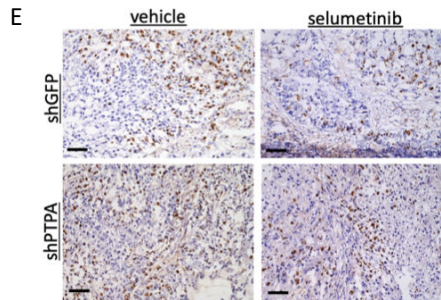
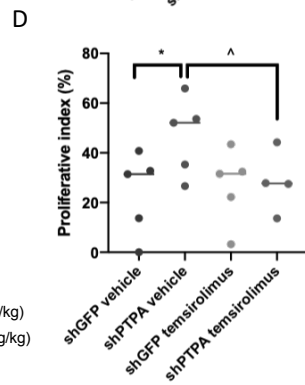
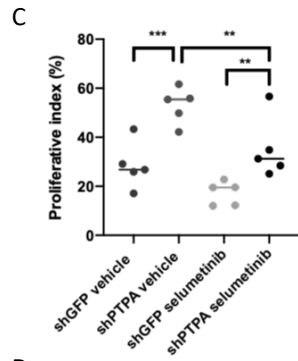
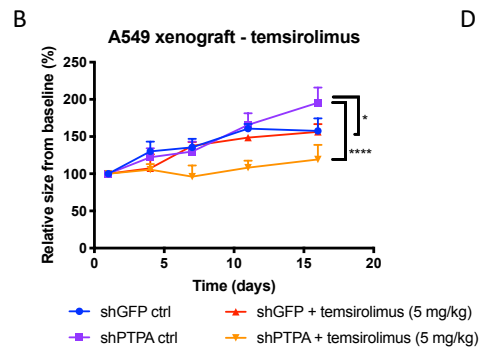
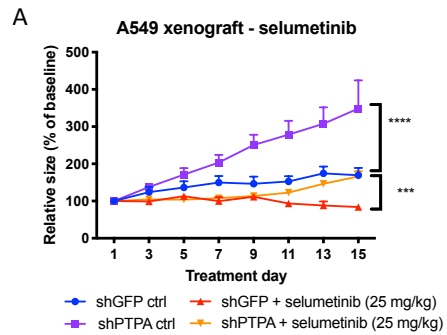


D

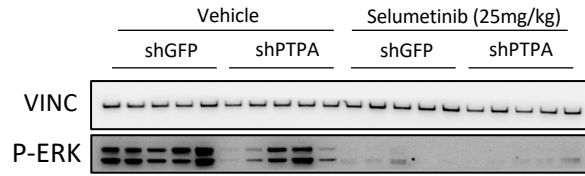


E

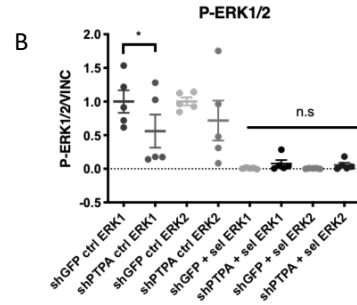




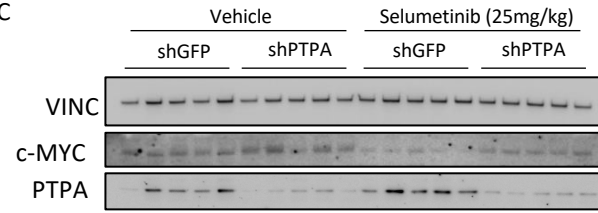
A



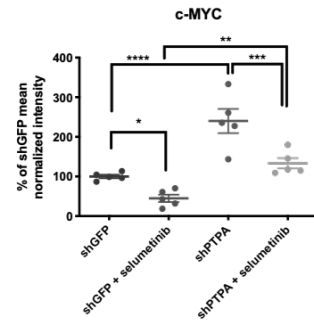
B

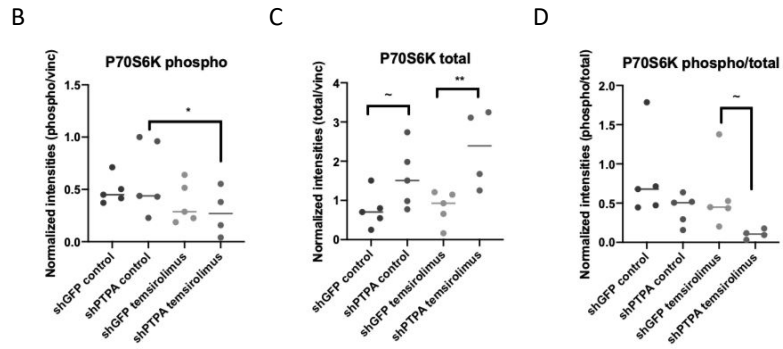
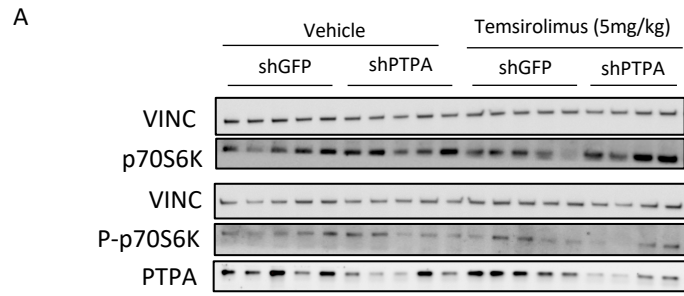


C



D





9. Supplementary Figures and Tables

Supplementary Figure 1:

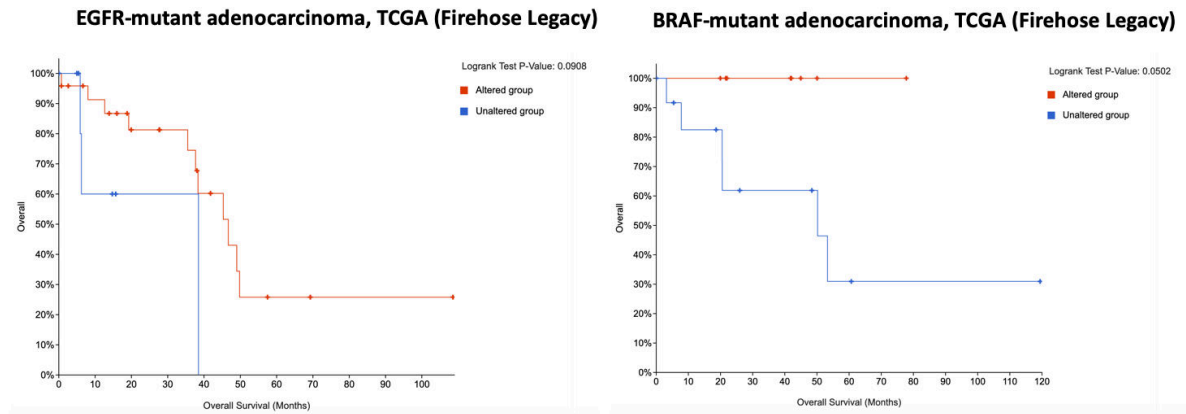


Figure S1: Kaplan-Meier survival data for EGFR-mutant (left panel) and BRAF-mutant non-small cell lung adenocarcinoma. Altered group: patients with PTPA heterozygous loss; Unaltered group: patients without PTPA heterozygous loss.

Supplementary Figure 2:

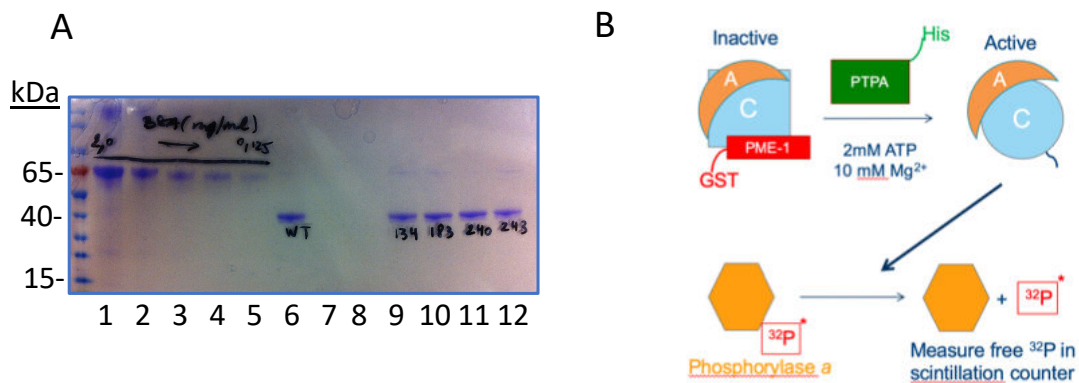


Figure S2: Purified recombinant His-PTPA wild-type and mutants used in phosphorylase α PP2A reactivation assay. **A:** Lane 1-5: 1/2 dilution series (20-1.25 μ g) of BSA. Lane 6: WT PTPA; Lane 9: R134W PTPA (not included in this manuscript). Lane 10: R183L PTPA. Lane 11: G240S PTPA. Lane 12: G243V PTPA. **B:** Schematic of PP2A reactivation assay. Inactive PP2A is isolated from HEK293T cells by PME-GST pull down using glutathione-Sepharose beads. Incubation with recombinant His-PTPA in the presence of ATP/Mg²⁺ activates PP2A, which can dephosphorylate a single radio-actively labeled phosphorylated residue on phosphorylase α .

Free radioactive phosphate detected by scintillation counting is a measure of PP2A activity and thus of PTPA functionality.

Supplementary Figure 3:

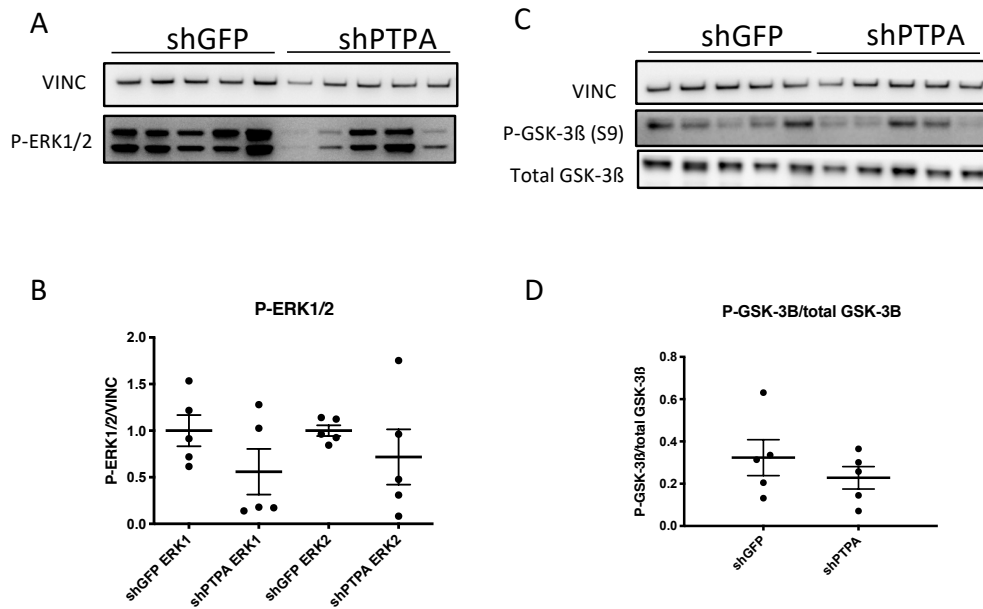


Figure S3: P-ERK1/2 and P-GSK-3β levels show no significant shPTPA-induced differences in A549 xenografts. **A,C:** Western blot analyses of P-ERK1/2 (**A**) and P-GSK-3β and total GSK-3β (**C**) in shGFP and shPTPA A549 xenografts. VINC: Vinculin. **B,D:** Quantifications of panel A (**B**) and panel C (**D**). Statistics: One-way ANOVA (**C**) and two-sided Student's t-test (**D**). Data are represented as mean +/- SEM. Differences in expression are non-significant for all conditions.

Supplementary Figure 4:

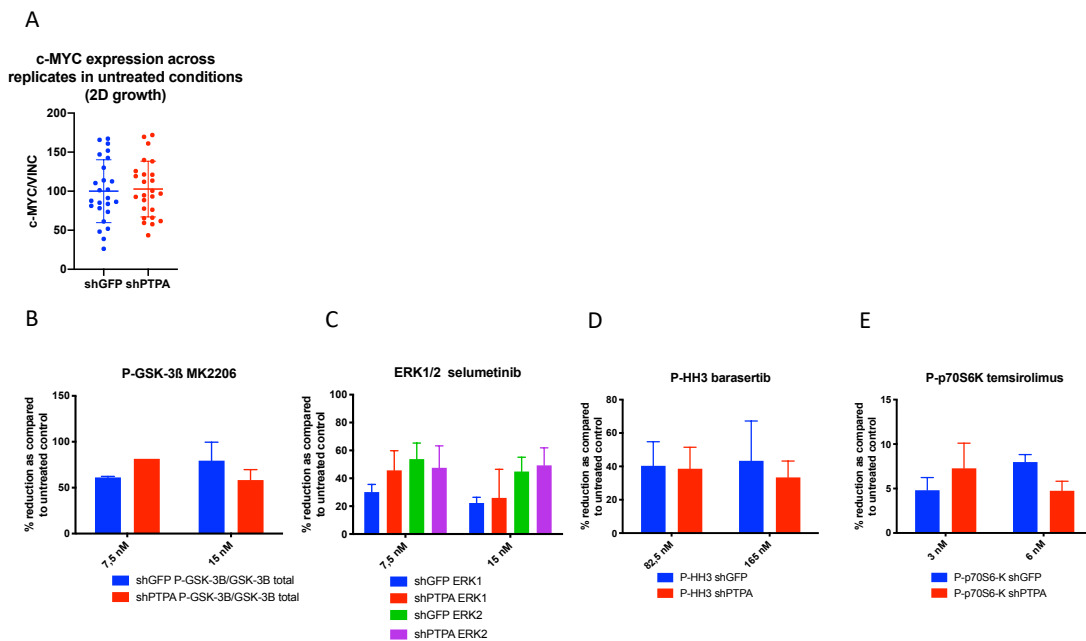


Figure S4: Quantifications of basal c-MYC levels, and P-GSK-3 β , P-ERK1/2, P-HH3 and P-p70S6K after treatments. A: Western blot analysis quantifications of c-MYC levels in untreated controls across technical and biological replicates. **B:** Western blot analysis quantifications of P-GSK3- β /total levels after MK2206 treatments (48 h) at indicated doses. **C:** Quantifications of Western blot images of P-ERK1/2 levels after selumetinib treatments (48 h) at indicated doses. **D:** Quantifications of Western blot images of P-HH3 levels after barasertib treatments (48 h) at indicated doses. **E:** Quantifications of Western blot images of P-p70S6K after temsirolimus treatment at indicated doses. Statistics: **A:** Two-sided Student's t-test. Data are represented as mean \pm SEM. **B-E:** Two-way ANOVA. Data are shown as mean \pm SEM. All statistical tests returned non-significant differences.

Supplementary Figure 5:

Supp fig S5:

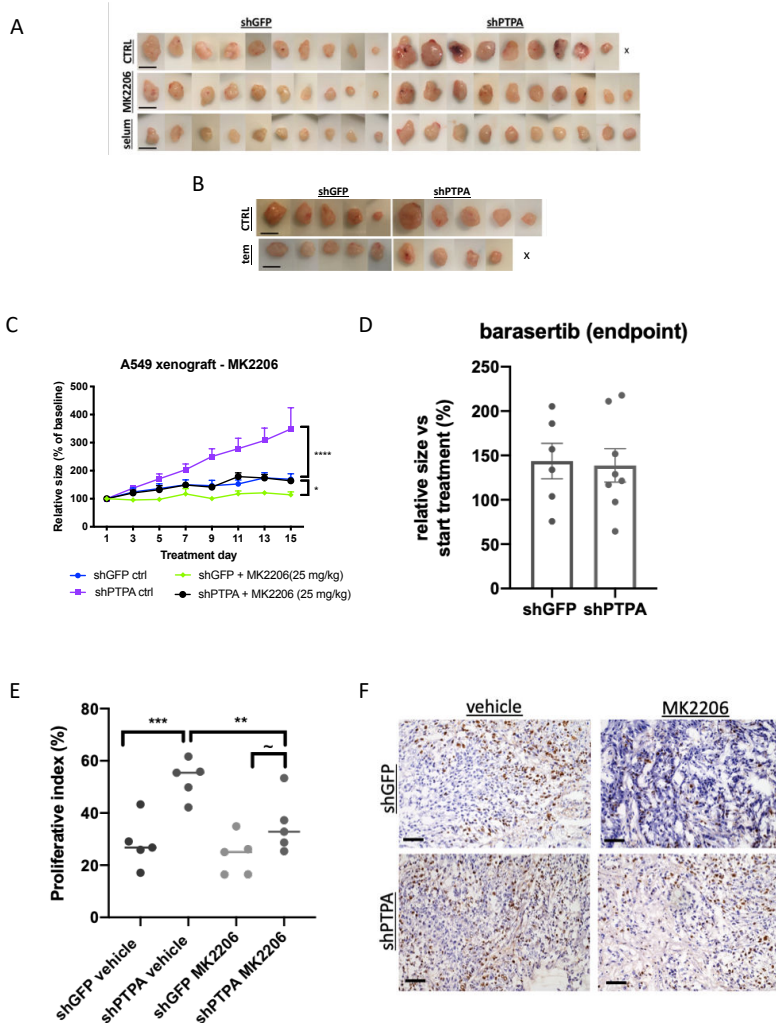


Figure S5: Images of excised tumors at treatment day 15.

A, B: Excised A549 shGFP and shPTPA xenografts after 15 days (25 mg/kg daily) for selumetinib and MK2206 and 16 days (5 mg/kg daily for 4 consecutive days followed by 2 days of rest). **A:** MK2206 and selumetinib treatment cohorts. **B:** Temsirolimus treatment cohorts. Scale bars represent 10 mm. CTRL: vehicle control; selum: selumetinib; tem: temsirolimus. **C:** MK2206 (25 mg/kg) tumor responses over time. Tumor sizes were normalized to size at treatment initiation. Statistics: 2-way ANOVA. *: $p < 0.05$; ****: $p < 0.0001$. **D:** Barasertib tumor responses after 15 days of treatment (50 mg/kg daily). No significant difference between shGFP and shPTPA was observed ($p = 0.9$). Tumor sizes were normalized to size at treatment initiation. **E:** Ki67 proliferative indices of MK2206 treatment and control cohorts. Statistics: One-way ANOVA. **: $p < 0.01$; ***: $p < 0.001$; ~: $p = 0.054$. **F:** Representative images of (E).

Supplementary Figure 6:

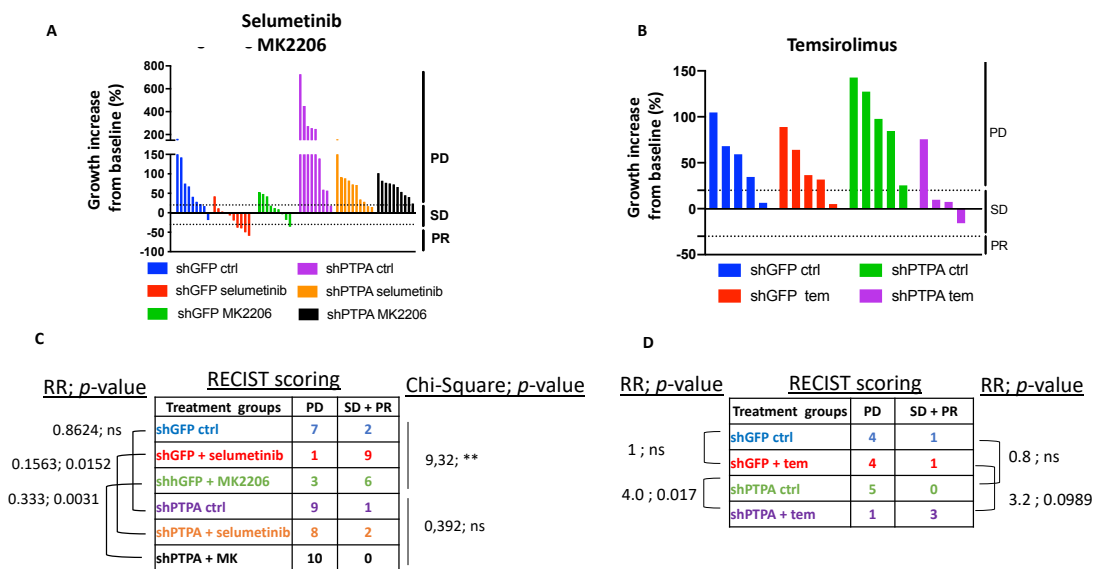


Figure S6: Adapted RECIST criteria further underscore the influence of PTPA on therapeutic outcomes against kinase inhibitors. A, B: Waterfall plots representing relative increase in size at endpoint, relative to treatment initiation. **A:** selumetinib and MK2206; **B:** temsirolimus. Responses were subdivided in Progressive Disease (>20% growth increase; **PD**), Partial Response (>30% growth reduction, **PR**) or Stable Disease (in between PD and PR; **SD**).

C,D: Contingency analysis of therapeutic responses against selumetinib and MK2206 (**B**) and temsirolimus (**C**). **RR:** relative risk. **C:** Loss of PTPA significantly deteriorated treatment outcomes against selumetinib and MK2206 (RR=0.15 and RR=0.333, resp.). **D:** Loss of PTPA improved outcomes against temsirolimus to a near significant extent (RR=3.2, $p=0.0989$), while it was the only therapy to significantly improve RECIST outcomes in the shPTPA depleted xenografts (RR=4.0). On the contrary, selumetinib and MK2206 were more effective in the PTPA wild-type setting as compared to temsirolimus (**C**). Statistics: Fisher-exact (C, D) and Chi-Square (C) test. SD and PR were pooled (SD+PR) in order to obtain sufficiently large groups for proper statistical analysis.

I. Supplementary Table 1: List of site-directed mutagenesis primers

Mutation	Forward primer sequence	Reverse primer sequence
R148L (183)	5' ggg gaa ctc cac gct cat tga cta cgg cac 3'	5' gtg ccg tag tca atg agc gtg gag ttc ccc 3'
Y199C (234)	5' g aaa ctc cag aaa aca tgc agg atg gag cca gcc 3'	5' ggc tgg ctc cat cct gca tgt ttt ctg gag ttt c 3'
G205S (240)	5' gat gga gcc agc cag cag cca ggg agt g 3'	5' cac tcc ctg gct gct ggc tgg ctc cat c 3'
G208V (243)	5' cag ccg gca gcc agg tag tgt ggg gtc tgg at 3'	5' atc cag acc cca cac tac ctg gct gcc ggc tg 3'
E225*(E190*)	5' ttc aat cgg tac ctt tag gtt atg cgg aaa ctc 3'	5' gag ttt ccg cat aac cta aag gta ccg att gaa 3'
H306L(H271L)	5' ggc cca ttt gca gag ctc tcc aac cag ctg tgg 3'	5' cca cag ctg gtt gga gag ctc tgc aaa tgg gcc 3'
V316F(V281F)	5' gg aac atc agc gcc ttc cct tcc tgg tcc aaa 3'	5' ttt gga cca gga agg gaa ggc gct gat gtt cc 3'

II. Supplementary Table 2: list of antibodies

Target	Brand	Product number	Dilution
VINCULIN	Sigma	V9131	1:5000
PTPA	Santa Cruz	sc-81607	1:500
anti-PP2A C	Gift S. Dilworth	clone F2.5G4	1:1000
anti-FLAG	Sigma	F3165	1:10.000; 1:50 (IP)
c-MYC	Cell Signaling Technologies	#5605	1:1000
c-MYC P-S62	Abcam	ab78318	1:500
c-MYC P-T58	Abcam	ab185655	1:1000
ERK1/2 P-T202/Y204	Cell Signaling Technologies	#9101	1:1000
p70S6K P-T389	Cell Signaling Technologies	#9205	1:1000
Total p70S6K	Cell Signaling Technologies	#9202	1:1000
AKT P-S473	Cell Signaling Technologies	#9271	1:100
GSK-3 β	Cell Signaling Technologies	#9315	1:1000
GSK-3 β P-S9	Cell Signaling Technologies	#9323	1:1000
Secondary, anti-Mouse IgG	Agilent Technologies	P026002-2	1:3000
Secondary, anti-Rabbit IgG	Cell Signaling Technologies	#7074	1:3000
Ki67, human specific	Abcam	EPR3610	1:500 (IHC)
Ki67	Cell Signaling Technologies	#9129	1:80 (IHC)
CD45	BD Biosciences	Clone 30-F11	1:50 (IHC)
AlexaFluor488, anti-rabbit	Invitrogen		1:300 (IHC)
AlexaFluor647, anti-Rat	Jackson's Laboratories		1:300 (IHC)

III. Supplementary Table 3A: Kinase inhibitor information

<u>Compound</u>	<u>Alias</u>	<u>Vendor</u>	<u>Category number</u>	<u>Target</u>	<u>Applied concentrations (μM), <i>in vitro</i></u>	<u>Applied dose, <i>in vivo</i></u>
MK2206		Selleckchem	S1078	AKT	0,3 - 0,00004572474	25mg/kg
Selumetinib	AZD6624	Selleckchem	S1008	MEK	0,3 - 0,00004572474	25mg/kg
Palbociclib	PD-0332991	Selleckchem	S1116	CDK4/6	3,33 - 0,00152416	n/a
Volasertib	BI 6727	Selleckchem	S2235	PLK1,2,3	50 - 0,00762079	n/a
Dactolisib	BEZ235	Selleckchem	S1009	PI3K/mTOR	10 - 0,00152416	n/a
Ralimetinib	LY2228820	Selleckchem	S1494	p38	10 - 0,00152416	n/a
GSK461364		MedChemExpress	HY-50877	PLK1	0,1 - 0,0001524	n/a
Buparlisib	BKM120	Selleckchem	S2247	PI3K	10 - 0,00152416	n/a
Sorafenib	BAY 43-9006	Selleckchem	S7397	Raf-1, others	10 - 0,00152416	n/a
Alisertib	MLN8237	Selleckchem	S1133	AURKA	3,33 - 0,00152416	n/a
SNS032	BMS-387032	Selleckchem	S1145	CDK2/7/9	10 - 0,00152416	n/a
Erlotinib	CP358774	Selleckchem	S1023	EGFR	3,33 - 0,00152416	n/a
Crizotinib	PF-02341066	Selleckchem	S1068	c-MET, ALK	10 - 0,00152416	n/a
BI2536		Selleckchem	S1109	PLK1,2,3	50 - 0,00762079	n/a
Ro3306		Tocris	4181	CDK1	30 - 0,004572474	n/a
Adavosertib	MK1755	Selleckchem	S1525	Wee1	10 - 0,00152416	n/a
Barasertib	AZD1152	MedChemExpress	HY-10127	AURKB	3,33 - 0,00152416	50 mg/kg
Temsirolimus	CCI-779	Selleckchem	S1044	mTOR	0,120 - 0,01828989	5 mg/kg

IV. Supplementary Table 3B: kinase inhibitors and relevant references

Compound	Target	References (PMID)	
		PP2A	MYC
MK2206	AKT	18042541; 30132971; 27531894	23331925; 11018017; 16788862; 33259779; 30132971
Selumetinib	MEK	16456541; 30021885;	30021885; 24685132; 16899113; 11018017; 28179307; 23639941; 21628402
Palbociclib	CDK4/6	23634261	28978620; 32934206; 31727874; 28978620; 24444383; 12070150; 10373516; 21885567;
Volasertib	PLK1,2,3	17121863; 21874008; 21252232	31571905, 29383095; 30217967; 23887393; 27699933; 32468878
Dactolisib	PI3K/mTOR	28199842; 27485451; (26459601) ; 26310906; 26118661 ; 25438055; 20227368; 19553685; 18056704; 11948686; 10200280; 30132971	21876152; 22363436; 27913436; 16788862; 22340590;
Ralimetinib	p38	15569672; 24015987 ; 15972258; 11259586 ; 18039929	28460458; 27913436; 15078869; 12819782; 11408569; 15634685
GSK461364	PLK1	17121863; 21874008; 21252232	31571905, 29383095; 30217967; 23887393; 27699933;
Buparlisib	PI3K		21876152; 22363436; 27913436; 16788862; 32068318; 22340590
Sorafenib	Raf-1, others	28161506; 19933846; 16239230; 15664191; 12932319; 11494123; 10801873; 21822300	19647225; 9464539; 2557616; 31980175; 29212027; 24934810; 24469106; 22836754; 21822300; 18679422; 11466616; 25128497; 24309997; 32559715
Alisertib	AURKA	24825897	30226440; 25284017; 20519624
SNS032	CDK2/7/9	28137908; 26253406; 18276582; 15122341; 16048649	28665315; 20818171; 19966300; 20010815; 20445224; 20713526; 18206647; 18206647; 11060032; 10409725; 9188852; 9163430; 9119229; 8386381; 25490451; 8065309; 29507396; 32645016; 31311847; 31243099; 29588524; 23776131; 21885567
Erlotinib	EGFR	30830869; 27821484; 24954871; 23178652; 19825976;	24922639; 30770740
Crizotinib	c-MET, ALK	30224486; 15075332;	29507657; 31776900; 31462708; 30290287; 12213716
BI2536	PLK1,2,3	17121863; 21874008; 21252232	31571905, 29383095; 30217967; 23887393; 27699933;
Ro3306	CDK1	32900880; 32591484; 26053095; 24616226; 19793917; 18056802; 23672858; 18056802; 23790971; 7622588	28665315; 31822694; 24444383; 18206647; 29512702; 28665315; 23776131; 21885567; 17589519;
Adavosertib	Wee1	33108758; 21849476; 18056802; 23790971	32195191; 31919076; 32049046; 32195191
Barasertib	AURKB	31527146; 26906715; 12082625; 25892238; 23789096; 23746640; 23345399; 23079597; 21874008;	25739120; 32049046; 25411027; 20519624; 19287963; 30540594
Temsirolimus	mTOR	28199842; 27485451; (26459601) ; 26310906; 26118661 ; 25925585; 20227368; 19553685; 18056704; 11948686; 10200280; 30132971	25925585; 33443202; 33259779; 32615570; 30733194; 30705387; 30568499; 30389701; 30132971; 30061153; 28978620; 28370287; 28174256; 23887393; 25537515; 26459601; 25999153; 27822418; 26459601; 25797247; 25537515; 24140020; 23242809; 21135252; 19773438; 19342893; 15634685; 14576155; 9715279

Searched Pubmed for: "PP2A" AND "target", "PP2A" AND "compound"; "MYC" AND "target", "MYC" AND "compound"